Patient-derived vascularized skin organoids unravel the role of systemic sclerosis fibroblasts in microvascular dysfunction.

Amandine PITAVAL[1†], Lara JOBEILI[1†], Caroline WELSCH[1], Stéphanie COMBE[1], Anastasia PAPOZ[1], Laure GIBOT[2], Matthieu ROUSTIT[3,4], Jean-Luc CRACOWSKI[3], Charles COUTTON[5], Xavier GIDROL[1*], Walid RACHIDI[1*]

[1] Univ. Grenoble Alpes, CEA, Inserm UA13, IRIG, BGE, Biomics, 38000, Grenoble, France.

[2] Univ. Toulouse, CNRS UMR 5623, Laboratoire Softmat, 31062, Toulouse, France.

[3] Univ. Grenoble Alpes, Inserm U1300, HP2, 38000, Grenoble, France.

[4] Univ. Grenoble Alpes, Inserm CIC1406, CHU Grenoble Alpes, 38000, Grenoble, France.

[5] Univ. Grenoble Alpes, Inserm U1209, CNRS UMR 5309, Institute for Advanced Biosciences, Team Genetics Epigenetics and Therapies of Infertility, 38000, Grenoble, France.

[†]These authors contributed equally to this work.

*Corresponding authors

walid.rachidi@cea.fr

xavier.gidro@cea.fr

Abstract

Systemic sclerosis (SSc) is a complex and poorly understood disease affecting connective tissue. Patients with SSc may suffer from painful digital ulcers due to endothelial cell dysfunction and excessive extracellular matrix production through fibroblast activation, leading to skin fibrosis.

To better understand the crosstalk between fibroblasts and endothelial cells in the context of SSc, we developed 3D vascularized skin organoids using SSc-derived fibroblasts from two patients.

After several morphological and molecular characterizations of healthy and pathological skin organoids, we demonstrate, for the first time, that SSc patient-derived fibroblasts can trigger structural abnormalities in skin organoids that emulate some features of the disease: the vasculopathy characterized by the formation of giant capillaries and the early fibrosis associated with cytokine and chemokine secretions. It appeared that SSc-derived fibroblasts play a major role in the vascular specificities of this disease, highlighting an interesting crosstalk between these cell populations. Therefore, these SSc-fibroblast containing skin organoids may enable to gain a deeper insight into the physiopathology of SSc and provide an alternative model to animal testing to evaluate the efficacy and safety of new drugs.

Keywords: limited cutaneous systemic sclerosis, vasculopathy, skin organoids, giant capillaries

Introduction

Systemic sclerosis (SSc) is a complex and poorly understood disease affecting connective tissue, characterized by excessive production of collagen matrix through fibroblast activation and an increase in the proportion of alpha-smooth muscle actin (αSMA)-expressing fibroblasts (myofibroblasts), leading over years to skin fibrosis and stiffness (Wynn 2007).

Complex interactions between endothelial cells, vascular smooth muscle cells, extracellular matrix (ECM), and circulating mediators contribute to the physiopathological setup of the disease. In the skin, vasculopathy is characterized by endothelial cell dysfunction associated with structural abnormalities such as a decrease in microvessel density and capillary dilatation named "giant capillaries". These early morphological changes precede the onset of fibrosis. Microangiopathy leads to digital ulcerations in more than one-third of patients and is responsible for pain, gangrene, and amputations (Asano and Sato 2015)·(Trojanowska 2010)·(Chora et al. 2015).

Preclinical studies on systemic sclerosis pathogenesis and therapeutics mostly rely on genetically engineered or chemically induced mouse models. However, none of the numerous mouse models available mimic the entire pathophysiology of the disease (Yue et al. 2018). In addition, conventional two-dimensional (2D) monolayer culture using fibroblasts derived from SSc biopsy samples cannot completely recapitulate SSc phenotypes when grown on plastic *in vitro* (Gardner et al. 2006). To overcome animal model limitations and 2D culture systems, 3D *in vitro* skin organoids have been recently developed to study the crosstalk between various cell types and their local microenvironment. Skin fibrotic disorders in human skin 3D models have been induced either chemically by TGF-β (Matei et al. 2019) or, more recently, by SSc-derived dermal fibroblasts (Huang et al. 2020) or SSc-derived keratinocytes (Russo et al. 2021). These models provide complementary 3D skin models. However, they could not investigate the causes of the vascular abnormality due to the lack of endothelial cells.

Classically, *in vitro* skin organoids (also known as reconstructed skin or skin substitutes) comprise a dermis colonized by fibroblasts and an epidermis composed of pluri-stratified layers of keratinocytes. However, such models constitute a simplified representation and lack the complexity of the human native skin that harbors multiple cell types and structures. Hence, scientists seek to increase skin organoid complexity at the physiological and cellular levels to better recapitulate dynamic cell/cell and cell/matrix interactions between the different cell types present in the skin. Considering the crucial role of cutaneous vascularization in oxygen and nutrient supply as well as thermoregulation, engineering vascularized skin organoids has become pivotal. Indeed, as this would enhance the long-term viability of the tissue (Auger, Gibot, and Lacroix 2013)·(Frueh et al. 2017) and also upgrade the skin organoid architecture to a more relevant system both physiologically and pathologically (Gibot et al. 2013)·(Matei et al. 2019)·(Jusoh, Ko, and Jeon 2019).

In the present study, we developed and characterized reproducible vascularized skin organoids. In our model, the dermal part comprised human primary dermal fibroblasts, endothelial cells (HUVECs: human umbilical vein endothelial cells) and adipose-derived stem cells (ADSCs); the epidermis was composed of human primary keratinocytes. All these cells could interact with each other in a physiological context. Then, we produced vascularized SSc skin organoids by substituting human primary dermal fibroblasts with SSc-derived dermal fibroblasts from two patients exhibiting different pathological features of limited cutaneous systemic sclerosis or Lc-SSC, a subtype of SSc characterized by skin fibrosis limited to the hands, forearms, face and feet. We investigated their crosstalk with healthy endothelial cells in a 3D context. Using an organoid skin model, we demonstrated the ability of SSc fibroblasts to induce vascular abnormalities (formation of giant capillaries), which recapitulate some of the earliest manifestations of this disease. These Lc-SSc skin organoids could be used as a preclinical model to evaluate the safety and efficacy of new drugs.

Results

Vascularized full-thickness skin organoids display a dermis rich in ECM, a mature endothelial network and a differentiated epidermis.

We generated and characterized vascularized skin organoids with N1-HDF (human primary fibroblasts derived from a healthy donor), GFP-expressing HUVECs, ADSCs and keratinocytes following the protocol described in the supplementary methods section (Figure 5A). For simplicity, only the origin of fibroblasts is indicated on the skin organoid images.

After 27 days of culture, hematoxylin-eosin saffron (HES) staining of paraffin sections highlighted the morphology of vascularized skin organoids. The results showed that these organoids properly mimicked human native skin architecture (Figure 1A). Two distinct cellular compartments were distinguishable: (1) the dermis with low cell density, dense ECM and the presence of a developed endothelial network and (2) the epidermis that appeared dense, highly organized, pluri-stratified, and differentiated, with all cell layers (basal, spinous, and granular layers as well as the stratum corneum) similar to native human skin. The epidermis homeostasis was monitored through filaggrin and cytokeratin 14 (CK14) expression as markers of terminal differentiation and basal keratinocyte proliferation, respectively (Figure 1B). The thickness of the epidermis in those organoids was 87 µm with a 95% CI of [81; 93] (Figure 1A/B). These results indicate proper basal cell proliferation and cell differentiation in the epidermis.

Immunostaining of laminin 332 and α6 integrin, two markers of the DEJ, confirmed the presence of an intact basement membrane. Their expression levels appeared qualitatively equivalent to that of native skin (Figure 1C).

Regarding the dermis composition, we focused on type I and type III collagen, two main components of the ECM secreted by fibroblasts (Figure 1D). Patterns of expression of type I and type III collagen were homogeneously distributed throughout the dermis and resembled the distribution observed in the native skin.

The generation and maturation of endothelial networks in vascularized skin organoids were both monitored with GFP-HUVECs using an inverted microscope. By D21 (during air-liquid interface), a dense, stable and interconnected endothelial network was detected (Figure 2A). The fluorescent labelling of CD31 (PECAM-1), a marker of endothelial cells, underlined the auto-organization of an endothelial network distributed in the whole dermis (Figure 2B). These capillaries contained a lumen (also observed in HES Figure 1A). The mean area of the endothelial lumen was 238 µm² with a 95% CI of [189; 288], representing 0.5% of the total dermis area (Figure 2C). The large dispersion was explained by the fact that vessels were cut either orthogonally or vertically into cross sections.

Alpha smooth muscle actin (αSMA) is a marker of both myofibroblasts and pericytes. In the dermis, αSMA-positive cells were mainly located in the upper layer of the dermis attesting to the presence of myofibroblasts in the papillary dermis (Figure 2B). Moreover, some αSMA-positive cells were aligned along capillaries and seemed to be in physical contact with them, suggesting that they were pericyte-like cells (Figure 2B). To ensure that αSMA constitutes a suitable pericyte marker, a supplemental staining of Calponin (pericyte marker) was used on successive cross-sections (Figure 2B). The colocalization between αSMA and Calponin confirmed that the cells surrounding capillaries were pericytes-like cells.

Around each capillary, there was on average 2.3 αSMA-positive cell / 100 μm^2 of vessel (data not shown). Interestingly, when the vessel area was sub-grouped by 200 µm², the vessel coverage of pericytes was 3.5 times higher on vessels whose area was below 200 µm² compared to larger vessels between 200 µm² and 400 µm² and more (Figure 2C).

Altogether, these observations indicate that vascularized skin organoids appear to recapitulate the main characteristics of native human skin: a structured epidermis, a normal DEJ, a dermis comprising a homogeneous ECM content, myofibroblasts and well-organized matured vessel-like structures with lumens and surrounded pericytes.

Vascularized skin organoids generated with patient-derived fibroblasts recapitulate some features observed in limited cutaneous systemic sclerosis skin.

Healthy and Lc-SSc vascularized skin organoids were generated with GFP-HUVECs, primary human ADSCs, primary human keratinocytes, and either primary dermal human fibroblasts derived from a healthy donor (N2-HDF) or two patients with limited cutaneous systemic sclerosis (SSc-HDF1 and SSc-HDF2) matched in sex and age (Table 2). Thus, in this study, we evaluated the capacity of our model to accurately recapitulate at least some phenotypical outcome of Lc-SSc using fibroblasts from those two patients.

After 27 days of culture, HES staining of paraffin sections highlighted the particular morphology of Lc-SSc vascularized skin organoids (Figure 3). For both healthy and pathological conditions, two cellular compartments were distinguishable: (1) the dermis with low cell density, dense ECM and the presence of a rich endothelial network; and (2) the epidermis that appeared dense, highly organized, pluri-stratified, and well differentiated. The thickness of the epidermis of pathological skin organoids was measured on HES staining (Figure 3A). The quantification revealed a slight yet significant decrease in the epidermis thickness for SSc-HDF2 compared to healthy N2-HDF. To further analyze the homeostasis of the epidermis, we monitored terminal differentiation and proliferation using filaggrin and CK14 expression, respectively. We did not observe any quantitative or qualitative differences among all three conditions (Figure 3B). These data indicate that using fibroblasts from Lc-SSc patients did not affect skin architecture except for the epidermis thickness in SSc-HDF2.

On the contrary, the DEJ was different between normal and Lc-SSc skin organoids (Figure 3C). Although laminin 332 and α6 integrin colocalized in all conditions, a statistically significant decrease in the expression of both proteins was observed in SSc-HDF2 compared to N2-HDF. In SSc-HDF1 however, there was an increase in laminin 332 expression but no significant difference in α6 integrin expression. These data demonstrate significant differences in the morphology of the DEJ depending on the origin of fibroblasts (and the clinical status) used to generate skin organoids, revealing a weaker DEJ in the case of SSc-HDF2 (presenting higher clinical severity).

The accumulation of excess extracellular matrix components such as collagen defines fibrosis, one of the SSc features. We therefore compared the ratio of collagen type III/I (a marker of connective tissue pathology) in the pathological skin organoids. At the time of analysis (27 days of culture), it did not significantly change between pathological and normal conditions (Figure 3D). In addition, myofibroblasts expressing αSMA were mainly located in the upper layer of the dermis (Figure 4B). No significant difference was observed among all three conditions (data not shown).

In Lc-SSc disease, several cytokines and chemokines have been implicated in the induction of fibrosis(Shima 2021). Their dysregulation plays a central role in initiating and maintaining inflammatory responses resulting in fibrosis and angiogenesis alterations (Randone et al. 2017). Using cytokine array, we assessed the relative level of human cytokine and chemokine secretions in the case of pathological skin organoids compared to the healthy control. Figure 3E shows a selection of the most secreted and differentially secreted cytokines between the healthy donor and the two pathological Lc-SSc. In the majority of cases, an increase of cytokine secretion was observed between SSc-HDF1 and SSc-HDF2 compared to N2-HDF but not significant. All cytokines were represented in the form of a heat map in Figure S1 and in a table (Table 3).

Altogether, these results indicate an effect of the SSc-HDF2 fibroblasts on the decrease of both epidermis thickness and DEJ integrity. Moreover, we did not observe any visible effect on collagen deposition with immunofluorescence nor on the myofibroblast number for both pathological conditions. However, cytokines and chemokines involved in SSc fibrosis were highly secreted in pathological models compared to healthy control indicating that this event likely precedes the fibrosis consisting in excessive production of collagen. Interestingly, some cytokines found to be higher in pathological conditions show a possible effect on the vascular network recapitulating the vasculopathy. Those results led us to investigate the endothelial network development in the three conditions.

Vascularized limited cutaneous systemic sclerosis skin organoids contain giant capillaries.

During culture at the air liquid interface until day 21, endothelial network was stable and interconnected (Figure 4A). Although it appeared denser with pathological fibroblasts, measurements of total tubule length and junction number showed no significant difference (Figure 4A).

HES staining of paraffin sections and immunofluorescence using CD31 highlighted the presence of a developed endothelial network and the presence of larger vessels in pathological conditions (Figure 3A, Figure 4B). Strikingly, the quantification on CD31-labelled sections showed that although the number of vascular structures did not change significantly between healthy and pathological skin organoids, the lumen area was significantly increased with SSc fibroblasts compared to healthy donor fibroblasts (Figure 4C, D). Interestingly, this effect was more pronounced for SSc-HDF2 than SSc-HDF1 (307 µm² with a 95% CI of [199; 416] for N2-HDF, and 528 µm² with a 95% CI of [360; 695] for SSc-HDF1 and 759 µm² with a 95% CI of [522; 997] for SSc-HDF2) (Figure 4C). These larger vessel-like structures are classically called "giant capillaries". In both conditions, they could reach a lumen surface of more than 6500 µm². Additionally, these larger vessel-like structures covered a higher dermis area than N2-HDF (Figure 4D). Indeed, the surface occupied by endothelial structures in the dermis was 1.5-fold higher for SSc-HDF1 and almost double in the case of SSc-HDF2 than for N2-HDF.

Around each vascular structure, the number of pericytes observed along vessels was quantified for each condition (Figure 4B, D). When the vessel area was classified into subgroups, we noticed that on vessels smaller than 200 μm^2, the pericyte coverage was significantly lower for SSc-HDF1 than N2-HDF. There were 3.2 αSMA-positive cells / 100 µm² of vessel for N2-HDF, 0.7 for SSc-HDF1, and 2.1 for SSc-HDF2. Overall, larger vessels with an area of more than 200 μm^2 were surrounded by very few pericytes, whatever the origin of the fibroblasts.

Altogether, we show for the first time that Lc-SSc fibroblasts substantially impact the organization of the endothelial network, leading to the formation of giant capillaries by a mechanism that remains to be identified. Hence, these networks resemble the “giant capillaries” observed in the dermis of SSc patients. This phenotypic outcome was stronger for SSc-HDF2 who displayed a higher clinical severity of the disease. Furthermore, these results suggest that these patient-derived vascularized skin organoids, as they recapitulate some critical features of the disease, could be used as a relevant model of systemic sclerosis to better understand the etiology of the disease regarding the vasculopathy or to screen drugs that could help patients.

Discussion

We generated vascularized skin organoids by growing fibroblasts/endothelial cells/keratinocytes and ADSCs in a fibrin hydrogel. Indeed, ADSCs, which can differentiate into pericyte-like cells, are commonly used to improve the stabilization of the endothelial network (Song et al. 2016)·(Andrée et al. 2019)·(Rohringer et al. 2014)·(Frueh et al. 2017). Moreover, ADSCs secrete several growth factors, such as cytokines and extracellular matrix components, important for numerous biological processes that control skin homeostasis (Metral et al. 2014). Under such conditions, we observed the development of a well-differentiated epidermis, stratified like a native human skin. Moreover, endothelial cells could self-organize into a functional vascular network within the dermis. CD31 staining of cross-sections revealed a *bona fide* vascular-like morphology containing a lumen and surrounded by pericytes-like cells. Furthermore, interactions between each cell type positively impacted vascular network organization and the generation of complex vascularized skin organoids.

We next aimed at generating vascularized skin organoids that partially model limited systemic sclerosis. This disease is characterized by a sequence of clinical manifestations. It begins with endothelial cell injury and vasculopathy, followed by B- and T-cell activation with exacerbated chemokine and cytokine production. These immune events lead to i) tissue inflammation and ii) hypoxia and fibroblast proliferation. The late clinical features include collagen accumulation, fibrosis, and progressive thickening and hardening of the skin ultimately resulting in ulceration. A 3D skin-like model with a self-assembled stroma containing SSc fibroblasts from patients with clinically diagnosed diffuse or limited cutaneous forms has previously been developed to highlight the role of SSc fibroblasts in TGFβ-induced fibrosis through LOXL4 regulation (Huang et al. 2020). Late characteristics of the disease, such as stromal contraction and increased tissue rigidity and collagen accumulation, have been described in SSc. In our model, after 27 days of culture, we did not observe any late-stage features of the disease including collagen accumulation, or an increase number of αSMA-expressing fibroblasts (Manetti et al. 2017)·(Robins et al. 2003). However, we detected the secretion of several cytokines known to play a significant role in the early initiation of the disease, such as Il-4, Il-6, and TNFα (Shima 2021). We also observed increased relative levels of some cytokines implicated in SSc-associated fibrosis and inflammation (GDF15, Il-8 (Randone et al. 2017), HGF (Kawaguchi et al. 2002)) and in vasculopathy (Angiopoietin-2 (Carvalheiro et al. 2020)) in both pathological

conditions. Together, these results suggest that the skin organoids we have generated with patient-derived fibroblasts recapitulate some early pathogenic events of the disease prior to overt fibrosis.

In addition, these donors suffered from a limited cutaneous SSc, characterized by a slight skin thickening and a small effect of skin fibrosis but a high disorganization of endothelial network compared to patients suffering from diffuse cutaneous SSc. In this study, fibroblasts originate from the diseased skin on the lateral face of the digits, which is an area well known for vascular abnormalities. In the physiopathology of SSc, endothelial alterations are described in patients before skin fibrosis due to the evolution of the disease from limited to diffuse over the years. Strikingly, the SSc skin models described here mimics the capillaroscopy pattern of the two Lc-SSc patients: the induction of "giant capillaries". This vascular defect could be due to the activation of apoptosis in endothelial cells (Chora et al. 2015)(Trojanowska 2010). Another possibility is that endothelial cells can undergo endo-mesenchymal transformation into myofibroblasts and produce more collagen (Trojanowska 2010),(Manetti et al. 2017), leading to intravascular fibrosis (Tsou et al. 2021). We seeded all fibroblasts from Lc-SSc patients and normal endothelial cells (HUVECs) in a hydrogel where they were able to self-assemble and self-organize.
Here, we show, for the first time, that Lc-SSc derived fibroblasts could directly induce defects in the microvascular network which display some specific features (giant capillaries) actually observed in the early stage of the pathology in the two donors used in this study.
In addition, pericytes were scattered on vessels with a surface area of more than 200 μm^2, recapitulating artery-like structures. This makes sense since one of the functions of pericytes is to act on the contraction of the endothelial network to regulate vascular diameter and capillary blood flow. However, these pericytes were more present on smaller vessels (mimicking capillary-like structures).

Of note, when using fibroblasts SSc-HDF2, we observed a lower expression of two DEJ proteins: laminin-332 and alpha6 integrin. To the best of our knowledge, only one study has reported a similar disruption of the DEJ in SSc skin (Abignano et al. 2013).

Among the limitations of our model, we did not observe any abnormalities in the epidermis, possibly because keratinocytes were derived from a young donor following breast surgery. In contrast, in a 3D epidermal model generated from keratinocytes obtained from SSc patients, keratinocyte activation and altered differentiation are both shown in fibrotic diseases or scars (Russo et al. 2021),(N. Aden et al. 2008),(Nima Aden et al. 2010),(Nikitorowicz-Buniak et al. 2014). Keratinocytes derived from SSc patients also induced differential expression of some ECM proteins in the dermis (McCoy et al. 2017),(Nima Aden et al. 2010). In their model, keratinocytes recapitulated the phenotype of the Lc-SSc epidermis with aberrant differentiation and a decrease in proliferation, strongly supporting that SSc keratinocytes display cell-intrinsic abnormalities (Russo et al. 2021). However, keratinocytes are not the major players in SSc pathophysiology.

Another limitation is that in this study we had a small number of Lc-SSc individuals with heterogeneous disease manifestations. In the future we need to increase the number of donors to determine whether similar changes occur across the variety of SSc disease subsets and to address the enormous inter-individual variations(Buechler et al. 2021) and to go deeper into the molecular mechanisms involved.

Conclusion

Here, we present a complex 3D vascularized human skin organoid model generated with fibroblasts derived from two Lc-SSc patients, who recapitulate some earlier features of the disease, such as secretion of cytokines preceding fibrosis, and microvasculopathy (Figure 5B). This bioengineered vascularized skin using primary fibroblasts derived from patients, offer a robust model to unravel the role of Lc-SSc patient-derived fibroblasts in endothelial dysfunction and DEJ integrity. Finally, as it recapitulates early manifestations of the disease, this model could be very useful to screen drugs that could reduce or delay later deleterious symptoms of scleroderma disease.

Materials and Methods

Tissue harvesting and primary cell culture

Human primary fibroblasts called N1-HDF and human primary keratinocytes were extracted from healthy young subjects. Skin tissue explants were obtained from surgically discarded female breast specimens. N1-HDF used for development and optimization of skin organoids were isolated as previously described (Auxenfans et al. 2012) and cultured in Dulbecco's modified Eagle medium (DMEM) supplemented with 10% FBS (Pan Biotech). After separation of the epidermis from the dermis, keratinocytes were isolated as previously described (Auxenfans et al. 2012) and grown in KSFM culture medium. Collection and storage of human skin samples was declared to the French authorities and validated in the CODECOH DC-2008-444 document. All subjects gave written informed consent, and the study was performed in accordance with ethical guidelines.

Primary human pathological fibroblasts were isolated from skin biopsies harvested from diseased skin on the lateral face of the finger from two females with limited cutaneous systemic sclerosis (SSc-HDF1 and SSc-HDF2) and one age- and sex-matched healthy control subject (N2-HDF). Samples were collected during a clinical trial, including written informed consent and IRB approval. Human primary fibroblasts called N2-HDF came from a healthy, age- and gender-matched donor from the TRP study. All research protocols about the collection and use of fibroblasts derived from skin biopsies were approved by the French ministry (DC-2008-735). Fibroblasts were isolated using the explant method. The biopsies used for the culture of fibroblasts were immediately placed in Cytomax culture medium (Adgenix®). The sample was placed in a single-use petri dish, divided into several pieces using a scalpel, cut into small fragments, and placed in a CO_2 oven. The cells were monitored daily with an inverted microscope. When the growth appeared sufficient, the cell pellets were recovered in PBS with a cryoprotector (DMSO) for freezing in nitrogen.

ADSCs (adipose-derived stem cells) were extracted from adipose tissue discarded from abdominoplasty of anonymous healthy patients (biopredic ref GRA001) as previously described (Bunnell et al. 2008).

The endothelial cells were GFP-expressing HUVECs (human umbilical vein endothelial cells) (cAP-0001GFP Angioproteomie) cultivated according to manufacturer recommendations.

Each cell type was cultured in a CO_2 incubator at 37 °C, and the appropriate culture medium was changed three times per week before confluence was reached. For passage, cells were rinsed with PBS solution twice and incubated with trypsin-EDTA 0.05% (Thermo Fisher Scientific, Waltham, MA, USA) for 5 min. They were subsequently incubated with a 10% FBS solution and centrifuged at 300 g for 5 min prior to resuspension in fresh culture media and subsequent culture.

In vitro, 3D vascularized human skin organoid preparation

Cell-laden hydrogel preparation and deposition:

For all experiments, a 2.5% (w/v) fibrinogen (F8630 Sigma–Aldrich) solution containing aprotinin (A6279 Sigma–Aldrich) and 2.5 mM $CaCl_2$ (C8106 Sigma–Aldrich) was prepared.

To establish vascularized dermal equivalents, experiments were carried out as follows (Figure 5A):

Fibroblasts (0.9 x 10^6 cells), GFP-HUVECs (0.4 x 10^6 cells) and ADSCs (0.3 x 10^6 cells) were added to 1 ml of fibrinogen solution.

After the addition of thrombin (T4648 Sigma–Aldrich) at a concentration of 1 U/ml, 360 µl of cell-laden hydrogel were immediately and carefully pipetted and deposited into each culture chamber (ref 3460 Transwell Corning) located in a 12-well plate and placed at 37 °C in an incubator containing 5% CO_2 for 30 min. Two ml of a mixture of 1:1 medium composed of DMEM (ref 31966047 DMEM Gibco, Life Technologies Ldt. Paisley, UK) supplemented with 10% FBS, 100 units/ml penicillin, and 100 µg/ml streptomycin and CnT-ENDO (Cellntec, Berne, Switzerland) were then subsequently applied to the bottom of each insert and 500 µl to the top. During the incubation period (12 days), 80 µg/ml ascorbic acid (A8960-5g Sigma–Aldrich, St Louis, USA) and 10 ng/ml EGF (EGF; R&D Systems, Minneapolis, MN, USA) were added to the cell culture medium to allow the formation of a dermal equivalent.

On day 12, human primary keratinocytes at passage 1 were harvested, and 45 000 keratinocytes were seeded onto the dermal equivalent. Each skin organoid was cultured in immersed conditions for 5 days in a green-adapted medium(Black et al. 2005), changing the medium three times a week. On day 17, the skin organoid was raised at the air-liquid interface. To do so, the insert was removed from the 12-well plate and placed into a 12-well insert holder (657110 Dominique Dutscher, Brumath, France). Four milliliters of a simplified medium composed of DMEM supplemented with 8 mg/ml of bovine serum albumin (A2153-50G Sigma–Aldrich), 80 µg/mL L-ascorbic acid, and antibiotics was added below the insert so that the bottom of the organoid was in contact with the medium. The insert was cultured for 10 more days, changing the media three times a week to trigger the formation of a full-thickness skin equivalent.

Samples were harvested and either fixed in 4% neutral-buffered formalin overnight and embedded in paraffin after dehydration and xylene incubation or directly embedded in Tissue Tek compound and frozen at -20 °C for histological and immuno-histological analysis. Three replicates were produced under biological conditions. Native human skin was also added for histological analysis as a reference.

Live endothelial network

The endothelial network from GFP-expressing HUVECs developement was monitored at different time points during skin organoid formation, and images were captured using an AxioObserver optical microscope (ZEISS Axio Observer Z1). Image processing and analysis were performed using ImageJ software with the MBF plugin for microscopy (http://www.macbiophotonics.ca/imagej/, Research Service Branch, US National Institute of Health, United States), and the vascular network was quantified automatically by Angioquant software(Niemisto et al. 2005).

Histology and immunohistological analyses

To assess the histological morphology of the skin organoids, paraffin-embedded formalin-fixed samples or frozen OCT samples were cut into 5 µm and 8 µm sections, respectively. After dewaxing and rehydration, sections were stained with hematoxylin, eosin, and saffron (HES staining) on paraffin-embedded sections. For immunofluorescence, labelling was performed either on paraffin-embedded or frozen OCT sections. Air-dried 8 µm cryo-sections were either incubated in 4% PFA solution for 15 min then in 0,1% Triton X-100 (Sigma–Aldrich) for 4 min or incubated in cold acetone solution for 10 min, followed by 3% BSA PBS incubation for 1 h to block nonspecific binding sites. Then, the slides were incubated with the primary antibodies listed in Table 1 diluted in 1,5% BSA in PBS overnight at 4 °C followed by Cy3- or Cy5-conjugated secondary antibodies (Jackson ImmunoResearch) for 30 min at RT. Nuclear counterstaining using DAPI was carried out according to a routing protocol. For αSMA / CD31 and Calponin / Nestin labelling, paraffin-embedded sections were treated with heat-mediated antigen retrieval treatment prior to incubation with 3% BSA PBS before the addition of primary and secondary antibodies. Image acquisition was performed using a Zeiss microscope (ZEISS Axio Imager Z1) for immunofluorescence experiments.

Image analysis and processing

Image processing and analysis were performed using ImageJ. The living epidermal thickness, including all layers from the basal layer to stratum granulosum except the stratum corneum, was measured as the distance between the basement membrane to the stratum corneum on HES staining and expressed in µm on at least six fields per image and at least four images per sample. For analysis of type I and III collagen of the dermis, the fluorescently positive area, after setting a threshold, was automatically detected and segmented from other pixels and measured and normalized with the stromal nuclei number (except nuclei from vessel structure). Type I and III collagen intensities were analyzed in same field. The result was expressed as the ratio of type III collagen to type I collagen (type III/type I). Regarding CD31-positive vessel analysis, the area of each vessel was manually delineated and measured. The results represent the area of the vessel lumen and are expressed in μm^2. The vessel area and the vessel number were normalized to the dermis area.

For αSMA expressing cells analysis, positive cells were counted around each CD31-positive vessel and subsequently normalized by the corresponding vessel area. The values were multiplied by 100 to get the number of pericytes per 100 μm^2 of vessel. Finally, for DEJ (dermal epidermal junction), α6 integrin and laminin 332 were analyzed following the same process. The positive fluorescent area was automatically detected after setting a

specific threshold for each labelling and the batch of images. The results were expressed as intensity relative to the length of the DEJ (in µm manually measured).

Cytokine array

We used a human proteome profiler human XL cytokine array (ARY022B, R&D systems, Minneapolis, USA) according to the manufacturer's instruction. Conditioned media from the four mature skin organoids (comprising either N1-HDF, N2-HDF, SSc-HDF1 or SSc-HDF2) were collected at the air-liquid interface stage. Each kit contained four membranes and each spotted in duplicate with 105 different cytokine-specific antibodies. Arrays were imaged using a Chemidoc™ MP system (Bio-rad, Hercules, CA, USA). Pixel intensities of individual spots were quantified using Image J software (NIH, Bethesda, USA). For each antibody, the intensity of the two duplicated spots was first averaged. Background intensity was then subtracted and the resulting values were normalized to the mean intensity of the positive reference spots located at three corners of each membrane. For normalization, the mean intensity of the positive controls was set to 1, and all cytokine signals were expressed relative to this value. Two biological replicates were performed and signal intensities corresponding to the same antibody were finally averaged.

Statistical analysis

To compare multiple groups with one grouping variable, one-way ANOVA with multiple comparisons and Tuckey's correction was performed. Regarding the vessel area analysis, a non-parametric test was applied since the data did not have a normal distribution. Statistical analyses were performed using GraphPad Prism 6 (GraphPad Software Inc., La Jolla, CA, USA). Data were expressed as mean and 95% confidence interval (CI). Values lower than 0.05 were considered significant and referred to by asterisks throughout the manuscript as follows: *$p<0.05$, **$p<0.01$, ***$p<0.001$ and ****$p<0.0001$.

Data and materials availability

Upon request, the data generated in this study are available from the corresponding authors.

Conflict of Interest

The authors declare that they have no conflicts of interest

Acknowledgments

This work was supported by ANR grant (ANR-18-CE17-0017), by the French National Research Agency under the Investissements d'Avenir program (ANR-15-IDEX-02), by "CEA DRF-impulsion", and "CEA inflexion OoC" grants, and by ASF (Association Sclerodermique de France).

We gratefully acknowledge Delphine Freida and Frederique Kermarrec for ADSC cell extraction from adipose tissue. We also thank Rebecca Powell for her assistance with proofreading the manuscript.

Figure legends

Figure 1: Characterization of complex physiological full-thickness vascularized skin organoids generated with healthy donor derived fibroblast (N1-HDF), GFP-HUVECs, ADSCs and keratinocytes

To make the naming of the images easier, we have chosen to indicate only the origin of the fibroblasts (N1-HDF).

A/ Morphological aspects of normal human skin and skin organoids after hematoxylin-eosin-saffron (HES) staining of paraffin sections. Vascularized skin organoids were cultivated for 27 days. HES staining performed on cross-sections showed a dermis displaying endothelial structures (red stars) and a well-developed epidermis. With the higher magnification view of the epidermis, we observed a complete epidermal stratification with the four expected cell layers: basal, spinous, granulous layers and stratum corneum. Scale bar 25 µm. Right, quantification of the epidermis thickness is expressed in µm and was measured from the basal layer to the granular layer. 80 independent fields from three independent experiments (2 technical replicates for each experiment). Scale bars 100 µm. Regarding the graphs, values are given as the mean with 95% CI.

B/ Immunofluorescence staining of epidermal differentiation (Filaggrin: red) and proliferation (Cytokeratin 14: red). The dotted line indicates the dermal epidermal junction (DEJ). Scale bars 100 µm.

C/ Immunofluorescence staining of DEJ proteins: laminin 332 (green) and α6 integrin (red). Scale bars 50 µm.

D/ Immunofluorescence staining of type I (green) and III collagens (red) in the dermis. The dotted line indicates the DEJ. Scale bars 100 µm.

Nuclei were counterstained with DAPI (B, C, D).

Figure 2: Characterization of the endothelial network on vascularized skin organoids

A/ Image of an endothelial network development using GFP-HUVEC at day 21 (after 7 days of air-liquid interface) during skin organoid maturation. Perpendicular view from the bottom surface. Scale bar 200 µm.

B/ Immunofluorescence of vessel-like structures on vascularized skin organoids using CD31 labeling (red) and αSMA staining (green). Nuclei were counterstained with DAPI. Scale bars 100 µm. The dotted line indicates the DEJ. The picture on the right represents a higher magnification view of a vessel-like structure (area of 670 μm^2). Scale bar 25 µm.

Three serial sections with 3 different stainings. From the left to the right: αSMA (green)/CD31 (red); αSMA (green)/Calponin (red); Calponin (green)/Nestin (red). Scale bars 25 µm.

C/ Graph on the left: Quantification of vessel lumen area in μm^2 with a y axis in log10. 10 independent fields from three independent experiments (2 technical replicates for each experiment). Values are given as the mean with 95% CI. Graph on the right: Distribution of pericyte-like cells as a function of vessel area.

Figure 3: Characterization of complex pathological vascularized skin organoids generated with fibroblasts derived from two patients suffering from limited cutaneous systemic sclerosis or Lc-SSC. All skin organoids were generated with a combination of fibroblasts, GFP- HUVECs, adipose-derived stem cells (ADSCs) and keratinocytes.

To make the naming of the images easier, we have chosen to indicate only the origin of the fibroblasts (N2-HDF: healthy donor, SSc-HDF1: patient 1 with Lc-SSC, SSC-HDF2: patient 2 with Lc-SSC). HUVECs, ADSCs, and keratinocytes were not derived from patients suffering from Lc-SSC.

A/ Morphological aspects after HES staining on paraffin sections of vascularized skin organoids generated with fibroblasts from one healthy donor (N2-HDF) and from two patients suffering from Lc-SSC (SSc-HDF1 and SSc-HDF2). Skin organoids were cultivated for 27 days. Quantification of the thickness of the epidermis was expressed in µm and measured from the basal layer to the granular layer. 90 independent fields from three independent experiments (2 technical replicates for each experiment). Scale bars 100 µm. Red stars indicate endothelial structures.

B/ Immunofluorescence staining of epidermal differentiation (Filaggrin: red) and proliferation (Cytokeratin 14: red). The dotted line indicates the DEJ. Scale bars 100 µm.

C/ Immunofluorescence of DEJ proteins: laminin 332 (green) and α6 integrin (red) and quantification expressed as the intensity related to the DEJ length. 10 independent fields from three independent experiments (2 technical replicates for each experiment). Scale bars 50 µm.

D/ Immunofluorescence staining of type I (green) and type III collagen (red) in the dermis. The intensity quantification was as a ratio of expression (normalization relative to the dermis cell number). 15 independent fields from three independent experiments. The dotted line indicates the DEJ. Scale bars 100 µm.

Nuclei were counterstained with DAPI (B, C, D). Values of graphs are given as the mean with 95% CI (A, C, D).

E/ Assessment of cytokine levels in skin organoids with fibroblasts derived from patients suffering from Lc-SSC. Graph representing a selection of the most differentially secreted cytokines between the healthy donor and the two pathological Lc-SSc. One membrane of the two biological replicates of each condition are shown (mean±SD).

*p<0.05, **p<0.01, *** p<0.001, ****p<0.0001.

Figure 4: Characterization of the endothelial network on pathological vascularized skin organoids with SSc fibroblasts

A/ Endothelial network at day 21 (after 7 days of air-liquid interface) during skin maturation using GFP-HUVECs. The quantifications of total tubule length and junction number were performed at this time point (three independent experiments). Scale bars 200 µm

B/ Immunofluorescence of vessel-like structures on vascularized skin organoids using CD31 (red) and αSMA (green) staining. Nuclei were counterstained with DAPI. Scale bars 100 µm. The lower panels represent a higher magnification view of vessel- like structures. Scale bars 50 µm. The dotted line indicates the DEJ.

C/ Quantification of vessel lumen area in µm² (with a y axis in log10) for the healthy donor (N2-HDF) and for the two Lc-SSC patients (SSc-HDF1 and SSc-HDF2). 10 independent fields from three independent experiments (2 technical replicates for each experiment). Values are given as the mean with 95% CI. Graph on the right: Distribution of pericyte-like cell as a function of vessel area.

D/ Graphs from left to right representing the vessel number normalized to dermis area (values in %), the vessel area normalized to dermis area (values in %) and the distribution of pericyte-like cell as a function of vessel area. Quantification of 10 independent fields from three independent experiments (2 technical replicates for each experiment). Values are given as the mean with 95% CI.

*p<0.05, **p<0.01, *** p<0.001, ****p<0.0001.

Figure 5: Graphical abstract resuming methodology of vascularized skin organoid production and morphology based on histology analysis of healthy donor and two Lc-SSc patients (Created with BioRender.com. BioRender.com/f74t381)

A/ Schematic representation of the generation of vascularized skin organoids using fibrin hydrogel and time-point.

B/ Resume of morphology observed on histological sections with SSc-HDF1 patient presenting the "early" pattern (few giant capillaries and no obvious capillary loss) and SSc-HDF2 patient presenting the "active" pattern (frequent giant capillaries, slight disorganization of the capillary network).

Table 1: List of primary antibodies used in this study

Table 2: Clinical features of the healthy donor and the two Lc-SSc (limited cutaneous systemic sclerosis) patients

Table 3: Assessment of cytokine levels in skin organoids with fibroblasts derived from patients suffering from Lc-SSC. Data representing the mean value and the SD of all the secreted cytokines between the healthy donor and the two pathological Lc-SSc.

Supplementary Figure 1: **Assessment of cytokines relative levels in skin organoids with fibroblasts derived from patients suffering from Lc-SSC.** Heat map representing all the secreted cytokines between the healthy donor and the two pathological Lc-SSc.

References

Abignano, Giuseppina et al. 2013. "Virtual Skin Biopsy by Optical Coherence Tomography: The First Quantitative Imaging Biomarker for Scleroderma." *Annals of the Rheumatic Diseases* 72(11): 1845–51.

Aden, N. et al. 2008. "Proteomic Analysis of Scleroderma Lesional Skin Reveals Activated Wound Healing Phenotype of Epidermal Cell Layer." *Rheumatology* 47(12): 1754–60.

Aden, Nima et al. 2010. "Epithelial Cells Promote Fibroblast Activation via IL-1α in Systemic Sclerosis." *Journal of Investigative Dermatology* 130(9): 2191–2200. http://dx.doi.org/10.1038/jid.2010.120.

Andrée, Birgit et al. 2019. "Formation of Three-Dimensional Tubular Endothelial Cell Networks under Defined Serum-Free Cell Culture Conditions in Human Collagen Hydrogels." *Scientific Reports* 9(1): 1–11.

Asano, Yoshihide, and Shinichi Sato. 2015. "Vasculopathy in Scleroderma." *Seminars in Immunopathology* 37(5): 489–500.

Auger, François A., Laure Gibot, and Dan Lacroix. 2013. "The Pivotal Role of Vascularization in Tissue Engineering." *Annual Review of Biomedical Engineering* 15: 177–200

Auxenfans, C et al. 2012. "Adipose-Derived Stem Cells (ASCs) as a Source of Endothelial Cells in the Reconstruction of Endothelialized Skin Equivalents." *Journal of tissue engineering and regenerative medicine* 6: 512–18.

Black, Annie F. et al. 2005. "Optimization and Characterization of an Engineered Human Skin Equivalent." *Tissue Engineering* 11(5–6): 723–33.

Buechler, Matthew B. et al. 2021. "Cross-Tissue Organization of the Fibroblast Lineage." *Nature* 593(7860): 575–79. http://dx.doi.org/10.1038/s41586-021-03549-5.

Bunnell, Bruce et al. 2008. "Adipose-Derived Stem Cells: Isolation, Expansion and Differentiation." *Methods* 45(2): 115–20. https://www.ncbi.nlm.nih.gov/pmc/articles/PMC3624763/pdf/nihms412728.pdf.

Carvalheiro, Tiago et al. 2020. “Angiopoietin-2 Promotes Inflammatory Activation in Monocytes of Systemic Sclerosis Patients.” *International Journal of Molecular Sciences* 21(24): 1–10.

Chora, Inês et al. 2015. “Vascular Biomarkers and Correlation with Peripheral Vasculopathy in Systemic Sclerosis.” *Autoimmunity Reviews* 14(4): 314–22. http://dx.doi.org/10.1016/j.autrev.2014.12.001.

Frueh, Florian S. et al. 2017. “Current and Emerging Vascularization Strategies in Skin Tissue Engineering.” *Critical Reviews in Biotechnology* 37(5): 613–25.

Gardner, Humphrey et al. 2006. “Gene Profiling of Scleroderma Skin Reveals Robust Signatures of Disease That Are Imperfectly Reflected in the Transcript Profiles of Explanted Fibroblasts.” *Arthritis and Rheumatism* 54(6): 1961–73.

Gibot, Laure, Todd Galbraith, Jacques Huot, and François A. Auger. 2013. “Development of a Tridimensional Microvascularized Human Skin Substitute to Study Melanoma Biology.” *Clinical and Experimental Metastasis* 30(1): 83–90.

Huang, Mengqi et al. 2020. “Systemic Sclerosis Dermal Fibroblasts Induce Cutaneous Fibrosis Through Lysyl Oxidase–like 4: New Evidence From Three-Dimensional Skin-like Tissues.” *Arthritis and Rheumatology* 72(5): 791–801.

Jusoh, Norhana, Jihoon Ko, and Noo Li Jeon. 2019. “ Microfluidics-Based Skin Irritation Test Using in Vitro 3D Angiogenesis Platform .” *APL Bioengineering* 3(3): 036101.

Kawaguchi, Yasushi et al. 2002. “Expression of Hepatocyte Growth Factor and Its Receptor (c-Met) in Skin Fibroblasts from Patients with Systemic Sclerosis.” *Journal of Rheumatology* 29(9): 1877–83.

Manetti, Mirko et al. 2017. “Endothelial-to-Mesenchymal Transition Contributes to Endothelial Dysfunction and Dermal Fibrosis in Systemic Sclerosis.” *Annals of the Rheumatic Diseases* 76(5): 924–34.

Matei, Alexandru- Emil et al. 2019. “Vascularised Human Skin Equivalents as a Novel in Vitro Model of Skin Fibrosis and Platform for Testing of Antifibrotic Drugs.” *Annals of the Rheumatic Diseases* 78(12): 1686–92.

McCoy, Sara S. et al. 2017. “Scleroderma Keratinocytes Promote Fibroblast Activation Independent of Transforming Growth Factor Beta.” *Rheumatology (United Kingdom)* 56(11): 1970–81.

Metral, Elodie et al. 2014. “Adipose-Derived Stem Cells Promote Skin Homeostasis and Prevent Its Senescence in an In Vitro Skin Model.” *Journal of Stem Cell Research & Therapy* 04(04).

Niemisto, Antti et al. 2005. “Robust Quantification of in Vitro Angiogenesis Through Image Analysis.” *IEEE Transactions on medical Imaging* 24(4): 549–53.

Nikitorowicz-Buniak, Joanna et al. 2014. “Abnormally Differentiating Keratinocytes in the Epidermis of Systemic Sclerosis Patients Show Enhanced Secretion of CCN2 and S100A9.” *Journal of Investigative Dermatology* 134(11): 2693–2702. http://dx.doi.org/10.1038/jid.2014.253.

Randone, Silvia Bellando et al. 2017. “Angiostatic and Angiogenic Chemokines in Systemic Sclerosis: An Overview.” *Journal of Scleroderma and Related Disorders* 2(1): 1–10.

Robins, Simon P. et al. 2003. “Increased Skin Collagen Extractability and Proportions of Collagen Type III Are Not Normalized after 6 Months Healing of Human Excisional Wounds.” *Journal of Investigative Dermatology* 121(2): 267–72. http://dx.doi.org/10.1046/j.1523-1747.2003.12373.x.

Rohringer, Sabrina et al. 2014. “Mechanisms of Vasculogenesis in 3D Fibrin Matrices Mediated by the Interaction of Adipose-Derived Stem Cells and Endothelial Cells.” : 921–33.

Russo, Barbara et al. 2021. “Dysfunctional Keratinocytes Increase Dermal Inflammation in Systemic Sclerosis. Results from Tissue-engineered Scleroderma Epidermis.” *Arthritis & Rheumatology*.

Shima, Yoshihito. 2021. “Cytokines Involved in the Pathogenesis of SSc and Problems in the Development of Anti-Cytokine Therapy.” : 10.

Song, Young Hye et al. 2016. "Adipose-Derived Stem Cells Increase Angiogenesis through Matrix Metalloproteinase-Dependent Collagen Remodeling." *Integrative Biology (United Kingdom)* 8(2): 205–15.

Trojanowska, Maria. 2010. "Cellular and Molecular Aspects of Vascular Dysfunction in Systemic Sclerosis." *Nat rev Rhumatol* 2(5): 479–500.

Tsou, Pei Suen, Pamela J. Palisoc, Nicholas A. Flavahan, and Dinesh Khanna. 2021. "Dissecting the Cellular Mechanism of Prostacyclin Analog Iloprost in Reversing Vascular Dysfunction in Scleroderma." *Arthritis and Rheumatology* 73(3): 520–29.

Wynn, Thomas A. 2007. "Common and Unique Mechanisms Regulate Fibrosis in Various Fibroproliferative Diseases." *Journal of Clinical Investigation* 117(3): 524–29.

Yue, Xiaoyang, Xinhua Yu, Frank Petersen, and Gabriela Riemekasten. 2018. "Recent Advances in Mouse Models for Systemic Sclerosis." *Autoimmunity Reviews* 17(12): 1225–34. https://doi.org/10.1016/j.autrev.2018.06.013.

Figure 1

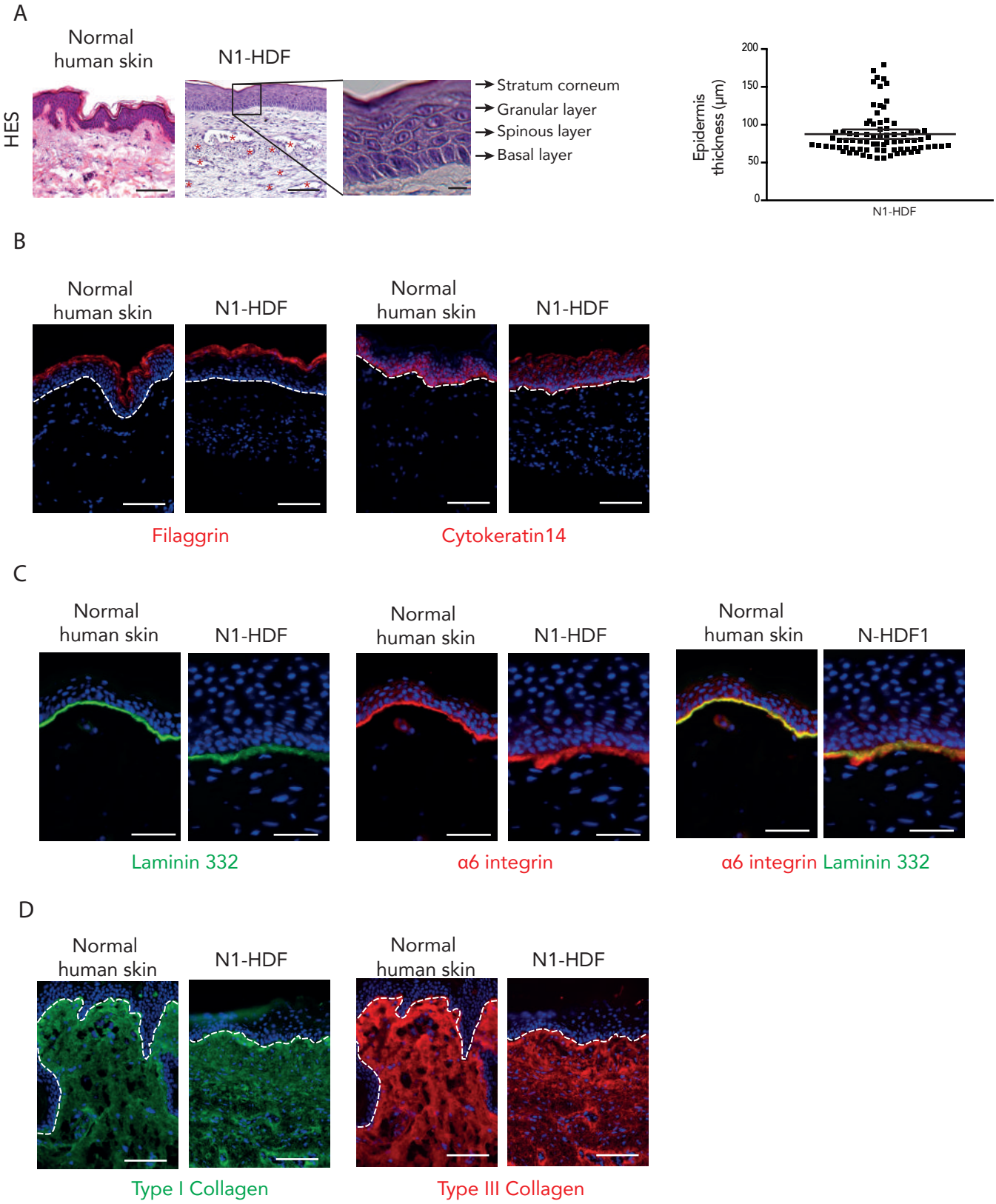
A
Normal human skin
N1-HDF
HES
Stratum corneum
Granular layer
Spinous layer
Basal layer
Epidermis thickness (µm)
200
150
100
50
0
N1-HDF
B
Normal human skin
N1-HDF
Normal human skin
N1-HDF
Filaggrin
Cytokeratin14
C
Normal human skin
N1-HDF
Normal human skin
N1-HDF
Normal human skin
N-HDF1
Laminin 332
α6 integrin
α6 integrin Laminin 332
D
Normal human skin
N1-HDF
Normal human skin
N1-HDF
Type I Collagen
Type III Collagen

Figure 2

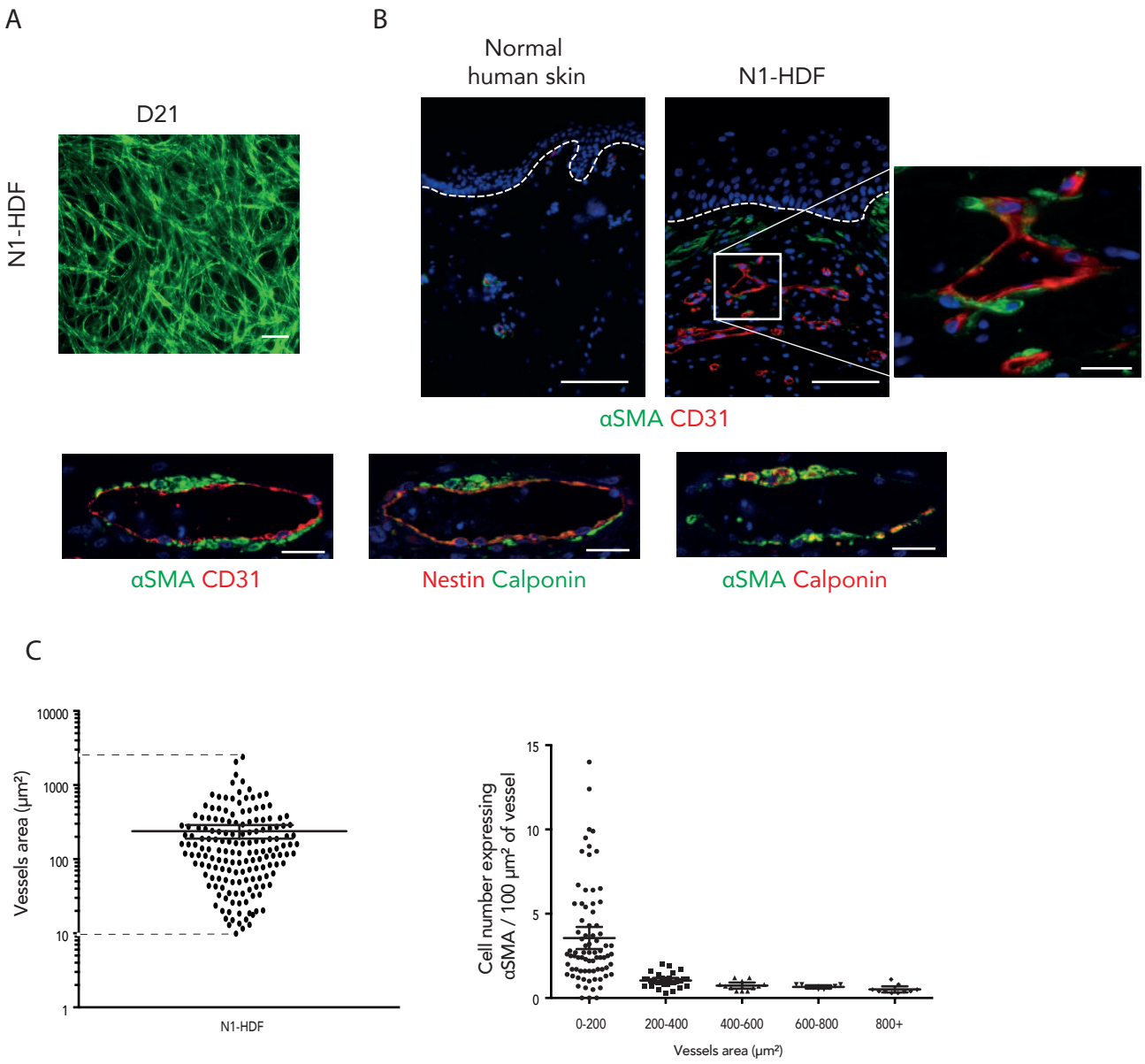
A
D21
N1-HDF
B
Normal
human skin
N1-HDF
αSMA CD31
αSMA CD31
Nestin Calponin
αSMA Calponin
C
Vessels area (µm²)
10000
1000
100
10
1
N1-HDF
Cell number expressing
αSMA / 100 µm² of vessel
15
10
5
0
0-200
200-400
400-600
600-800
800+
Vessels area (µm²)

Figure 3

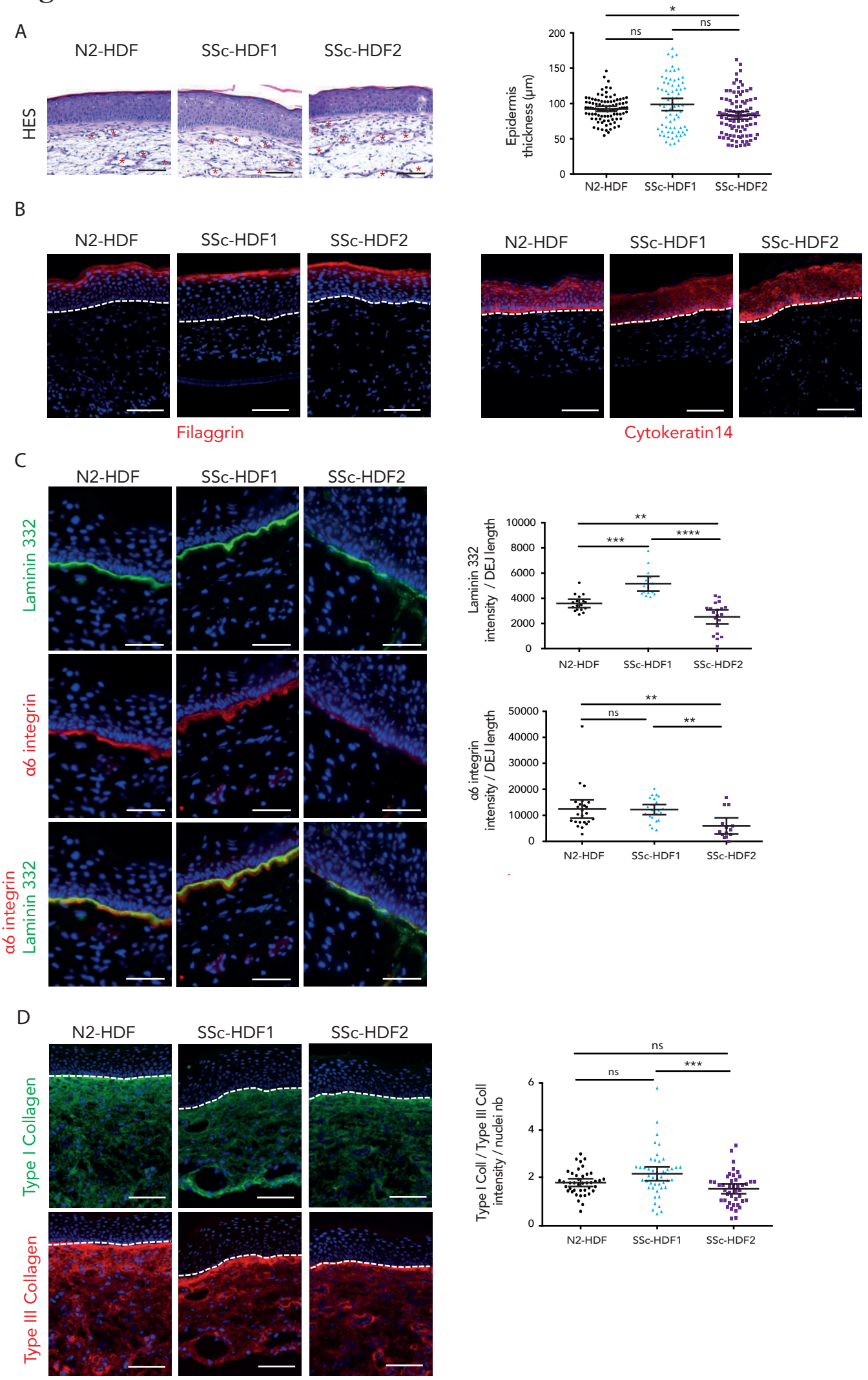
A
N2-HDF
SSc-HDF1
SSc-HDF2
HES
Epidermis thickness (µm)
200
150
100
50
0
ns
ns
*
N2-HDF
SSc-HDF1
SSc-HDF2
B
N2-HDF
SSc-HDF1
SSc-HDF2
Filaggrin
N2-HDF
SSc-HDF1
SSc-HDF2
Cytokeratin14
C
N2-HDF
SSc-HDF1
SSc-HDF2
Laminin 332
α6 integrin
α6 integrin
Laminin 332
Laminin 332 intensity / DEJ length
10000
8000
6000
4000
2000
0
**
***
****
N2-HDF
SSc-HDF1
SSc-HDF2
α6 integrin intensity / DEJ length
50000
40000
30000
20000
10000
0
**
ns
**
N2-HDF
SSc-HDF1
SSc-HDF2
D
N2-HDF
SSc-HDF1
SSc-HDF2
Type I Collagen
Type III Collagen
Type I Coll / Type III Coll intensity / nuclei nb
6
4
2
0
ns
ns
***
N2-HDF
SSc-HDF1
SSc-HDF2

E

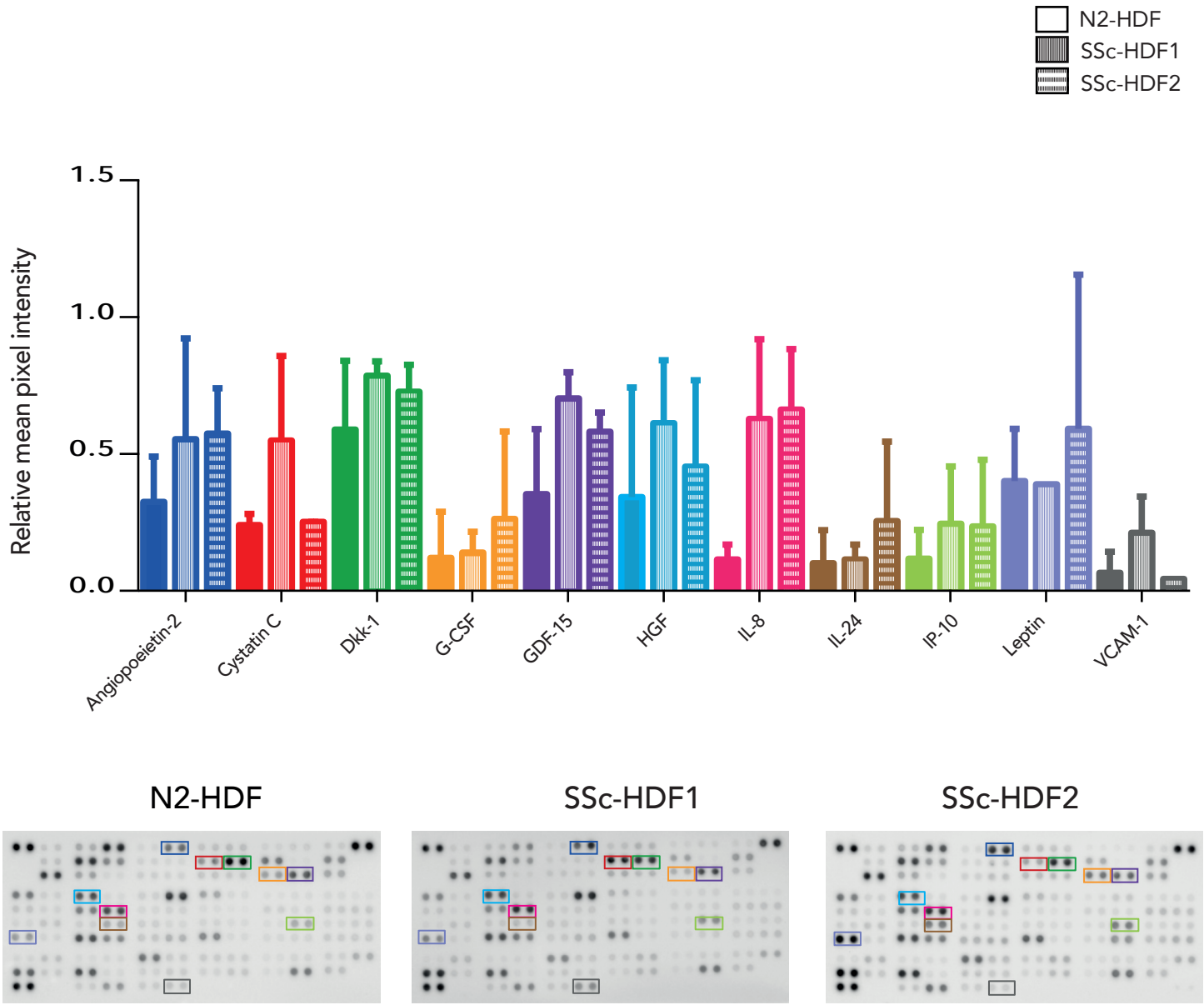
N2-HDF
SSc-HDF1
SSc-HDF2
Relative mean pixel intensity
1.5
1.0
0.5
0.0
Angiopoeietin-2
Cystatin C
Dkk-1
G-CSF
GDF-15
HGF
IL-8
IL-24
IP-10
Leptin
VCAM-1
N2-HDF
SSc-HDF1
SSc-HDF2

Figure 4

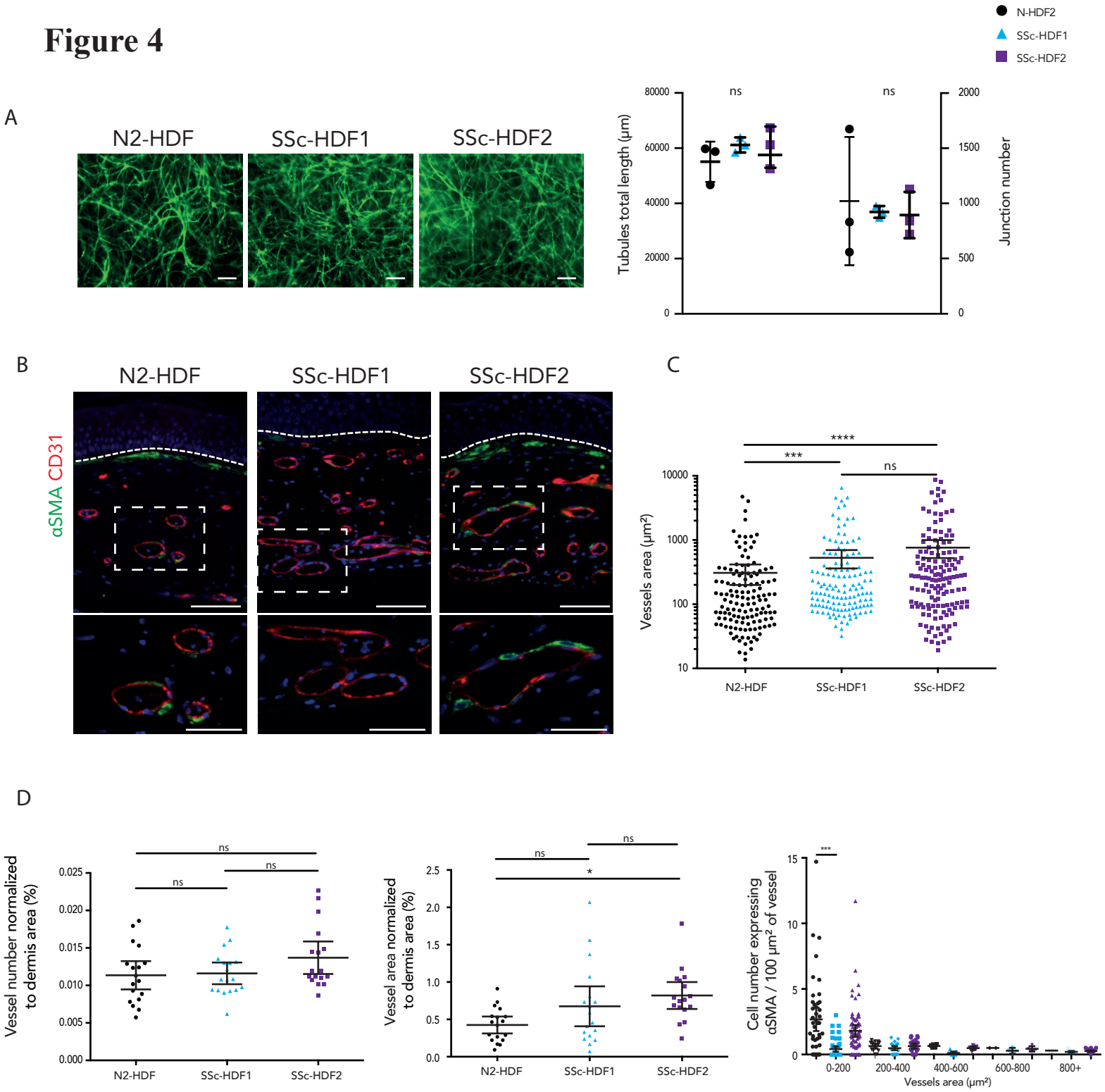
N-HDF2
SSc-HDF1
SSc-HDF2
A
N2-HDF
SSc-HDF1
SSc-HDF2
Tubules total length (µm)
Junction number
ns
ns
B
N2-HDF
SSc-HDF1
SSc-HDF2
αSMA CD31
C
Vessels area (µm²)
****
***
ns
N2-HDF
SSc-HDF1
SSc-HDF2
D
Vessel number normalized to dermis area (%)
Vessel area normalized to dermis area (%)
Cell number expressing αSMA / 100 µm² of vessel
Vessels area (µm²)
0-200
200-400
400-600
600-800
800+

A

VASCULARIZED SKIN ORGANOID PRODUCTION

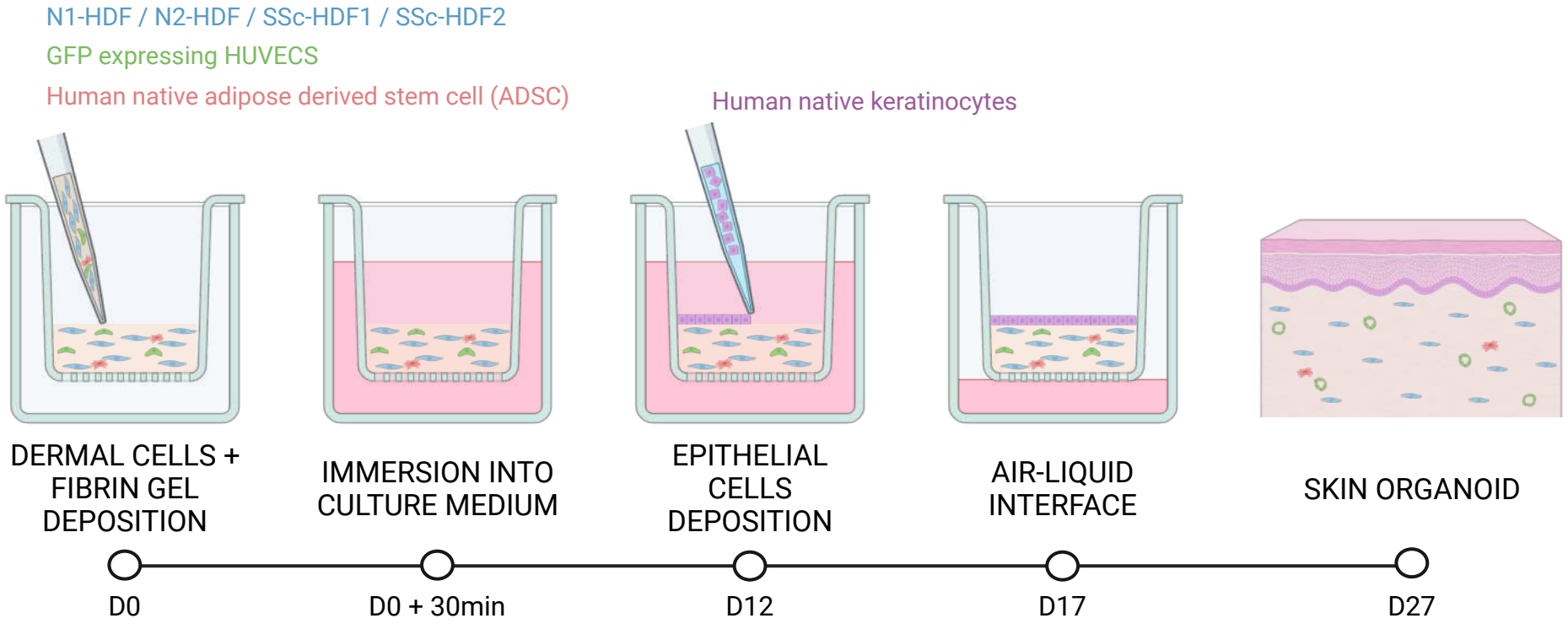

B

VASCULARIZED Lc-SSc SKIN ORGANOID MORPHOLOGY

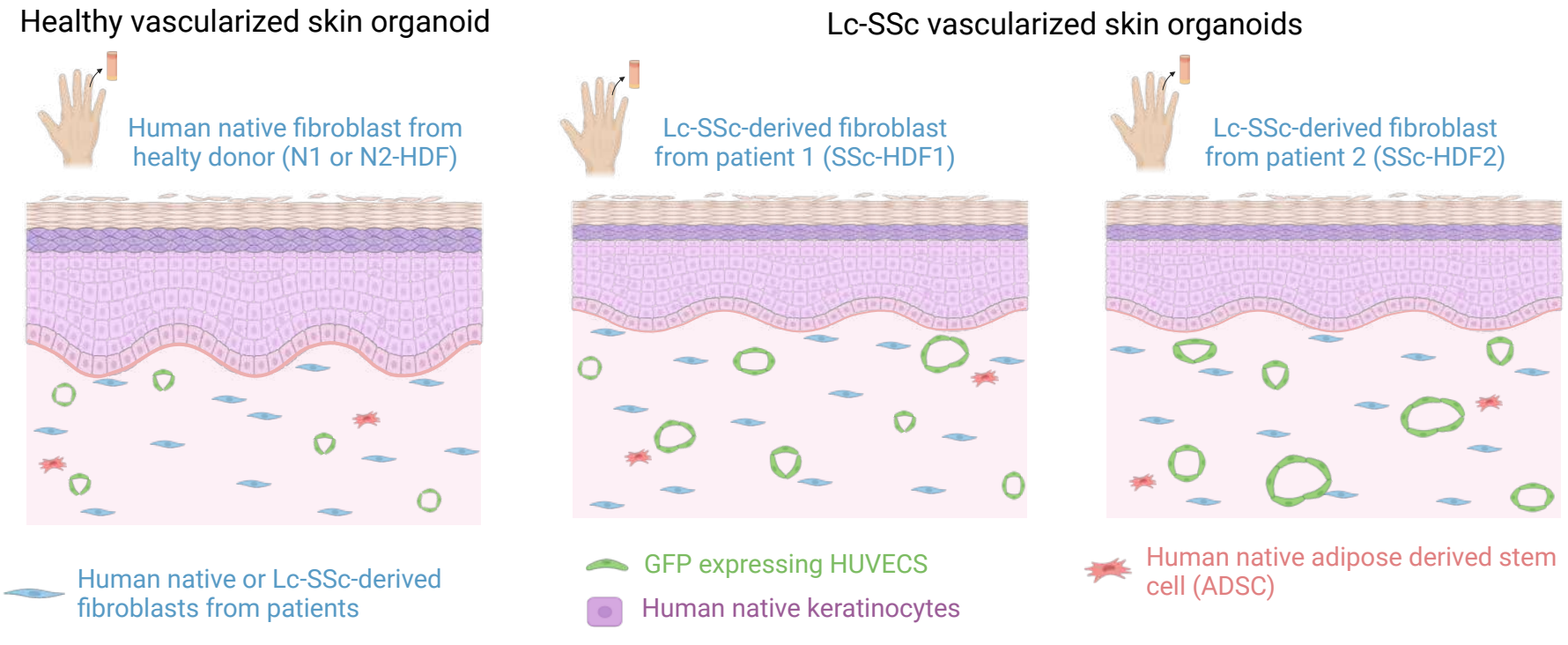

Table 1

Antibody	Clones/Reference	Company	Dilution	Fixation	Species
Cytokeratin 14	LL002	abcam	1/800	PFA	Mouse
Filaggrin	SPM181	abcam	1/100	PFA	Mouse
Laminin 332	P3H9-2	abcam	1/100	cold acetone	Mouse
Alpha 6 Integrin	NIK-GoH3	millipore	1/500	cold acetone	Rat
CD31	EP3095	abcam	1/400	cold acetone	Rabbit
Nestin	10C2	abcam	1/800	PFA	Mouse
Calponin	EP798Y	abcam	1/200	PFA	Rabbit
Alpha SMA	NCL-LSMA	novacastra leica	1/100	PFA	Mouse
Type I collagen	20111	novotec	1/250	cold acetone	Rabbit
Type III collagen	60315	novotec	1/1000	cold acetone	Mouse

Table 2

	N2-HDF	SSc1-HDF	SSc2-HDF
Age	54	54	54
Raynaud condition score (0-10)	0	5	5
Disease duration (years)	0	14	23
Modified Rodnan score (0-66) (proximal interphalangeal joint)	0	2	4
Cutulo pattern	0	Early (few megacapillaries)	Active (numerous megacapillaries)
Videocapillaroscopy	Normal	Abnormal	Abnormal

Table 3

	N2-HDF		SSc-HDF1		SSc-HDF2	
	mean	SD	mean	SD	mean	SD
Adiponectin	0,07	0,06	0,06	0,03	0,06	0,04
Apolipoprotein A-1	0,16	0,08	0,13	0,03	0,12	0,06
Angiogenin	0,69	0,09	0,46	0,08	0,57	0,12
Angiopoeietin-1	0,03	0,02	0,05	0,03	0,02	0,00
Angiopoeietin-2	0,33	0,17	0,55	0,37	0,57	0,17
BAFF	0,07	0,04	0,09	0,02	0,10	0,02
BDNF	0,07	0,07	0,12	0,05	0,07	0,02
Complement C5/C5a	0,03	0,04	0,04	0,01	0,01	0,02
CD14	0,04	0,05	0,06	0,00	0,01	0,03
CD30	0,05	0,07	0,05	0,01	0,03	0,02
CD40 ligand	0,08	0,06	0,06	0,02	0,05	0,03
Chitinase 3-like	0,66	0,11	0,65	0,06	0,68	0,06
Complement Factor D	0,32	0,01	0,28	0,01	0,29	0,01
C-Reactive protein	0,04	0,01	0,06	0,02	0,03	0,00
Cripto-1	0,02	0,02	0,05	0,03	0,06	0,07
Cystatin C	0,24	0,04	0,55	0,31	0,25	0,00
Dkk-1	0,59	0,25	0,79	0,05	0,73	0,10
DPPIV	0,25	0,28	0,23	0,05	0,19	0,02
EGF	0,02	0,02	0,03	0,02	0,01	0,03
Emmprin	0,21	0,21	0,30	0,06	0,28	0,15
ENA-78	0,71	0,01	0,75	0,07	0,77	0,05
Endoglin	0,17	0,12	0,16	0,09	0,14	0,13
Fas ligand	0,03	0,01	0,05	0,02	0,02	0,00
FGF basic	0,04	0,01	0,07	0,04	0,04	0,02
FGF-7	0,02	0,02	0,05	0,03	0,06	0,08
FGF-19	0,10	0,04	0,21	0,01	0,11	0,03
Flt-3 ligand	0,04	0,03	0,09	0,04	0,09	0,10
G-CSF	0,12	0,17	0,14	0,08	0,26	0,32
GDF-15	0,35	0,24	0,70	0,10	0,58	0,07
GM-CSF	0,12	0,16	0,12	0,06	0,15	0,17
GRO alpha	0,36	0,12	0,34	0,11	0,38	0,10
Growth hormone	0,04	0,04	0,04	0,04	0,03	0,02
HGF	0,34	0,40	0,61	0,23	0,45	0,32
ICAM-1	0,03	0,01	0,05	0,04	0,03	0,01
IFN gamma	0,04	0,02	0,05	0,04	0,03	0,02
IGFBP-2	0,52	0,22	0,62	0,34	0,53	0,32
IGFBP-3	0,24	0,00	0,11	0,08	0,21	0,07
IL-1 alpha	0,02	0,01	0,04	0,02	0,04	0,03
IL-1 beta	0,00	0,00	0,02	0,02	0,01	0,01
IL-1ra	0,01	0,01	0,03	0,01	0,05	0,05
IL-2	0,02	0,01	0,03	0,02	0,02	0,00
IL-3	0,01	0,01	0,02	0,01	0,02	0,01
IL-4	0,07	0,04	0,06	0,05	0,07	0,04
IL-5	0,03	0,04	0,02	0,02	0,01	0,01
IL-6	0,21	0,25	0,27	0,23	0,29	0,35
IL-8	0,53	0,04	0,63	0,29	0,66	0,22
IL-10	0,03	0,01	0,03	0,02	0,02	0,00
IL-11	0,04	0,01	0,05	0,02	0,05	0,02
IL-12 p70	0,02	0,00	0,03	0,01	0,01	0,01
IL-13	0,00	0,00	0,01	0,00	0,00	0,00
IL-15	0,03	0,03	0,03	0,01	0,03	0,02
IL-16	0,01	0,02	0,03	0,01	0,02	0,01
IL-17A	0,10	0,04	0,15	0,07	0,16	0,05

	N2-HDF		SSc-HDF1		SSc-HDF2	
	mean	SD	mean	SD	mean	SD
IL-18 Bpa	0,04	0,04	0,08	0,04	0,08	0,03
IL-19	0,03	0,02	0,02	0,01	0,03	0,02
IL-22	0,08	0,03	0,06	0,04	0,06	0,02
IL-23	0,03	0,04	0,05	0,05	0,03	0,03
IL-24	0,10	0,12	0,11	0,05	0,26	0,29
IL-27	0,04	0,03	0,04	0,04	0,02	0,02
IL-31	0,02	0,02	0,01	0,01	0,00	0,00
IL-32	0,03	0,02	0,04	0,04	0,02	0,02
IL-33	0,01	0,01	0,02	0,02	0,01	0,01
IL-34	0,01	0,01	0,01	0,00	0,01	0,00
IP-10	0,12	0,10	0,25	0,21	0,23	0,24
I-TAC	0,02	0,02	0,02	0,01	0,01	0,00
Kallikrein 3	0,04	0,03	0,04	0,00	0,03	0,01
Leptin	0,40	0,19	0,39	0,05	0,59	0,56
LIF	0,02	0,03	0,02	0,03	0,02	0,02
Lipocalin-2	0,55	0,02	0,60	0,23	0,59	0,11
MCP-1	0,31	0,11	0,36	0,14	0,37	0,07
MCP-3	0,05	0,04	0,04	0,02	0,07	0,09
M-CSF	0,14	0,01	0,10	0,06	0,09	0,03
MIF	0,38	0,02	0,36	0,24	0,38	0,26
MIG	0,02	0,01	0,02	0,03	0,01	0,01
MIP-1a/MIP-1b	0,01	0,01	0,01	0,01	0,02	0,01
MIP-3a	0,02	0,01	0,04	0,02	0,14	0,18
MIP-3b	0,03	0,03	0,04	0,04	0,04	0,04
MMP-9	0,04	0,03	0,10	0,04	0,08	0,03
Myeloperoxydase	0,02	0,03	0,03	0,02	0,02	0,02
Osteopontin	0,07	0,07	0,09	0,08	0,08	0,10
PDGF-AA	0,03	0,00	0,03	0,01	0,02	0,01
PDGF-AB/BB	0,02	0,02	0,01	0,00	0,01	0,01
Pentraxin 3	0,49	0,05	0,31	0,05	0,44	0,15
PF4	0,04	0,05	0,03	0,04	0,07	0,09
RAGE	0,04	0,05	0,03	0,05	0,04	0,04
RANTES	0,04	0,04	0,08	0,10	0,10	0,12
RBP-4	0,02	0,00	0,02	0,00	0,01	0,01
Relaxin-2	0,02	0,02	0,03	0,02	0,02	0,02
Resistin	0,05	0,02	0,05	0,01	0,04	0,01
SDF-1a	0,22	0,03	0,29	0,06	0,21	0,02
Serpin E1	0,67	0,17	0,84	0,13	0,93	0,21
SHBG	0,05	0,05	0,06	0,03	0,06	0,06
ST2	0,50	0,17	0,49	0,08	0,52	0,41
TARC	0,02	0,02	0,02	0,01	0,01	0,01
TFF3	0,04	0,02	0,04	0,01	0,06	0,06
TfR	0,04	0,04	0,03	0,01	0,05	0,05
TGF alpha	0,03	0,03	0,02	0,02	0,02	0,02
Thrombospondin-1	0,06	0,04	0,10	0,05	0,09	0,05
TNF alpha	0,01	0,01	0,02	0,02	0,01	0,01
uPAR	0,27	0,23	0,34	0,27	0,33	0,20
VEGF	0,09	0,05	0,08	0,04	0,07	0,06
Vitamin D BP	0,06	0,03	0,07	0,04	0,06	0,05
CD31	0,22	0,11	0,22	0,06	0,33	0,25
TIM-3	0,04	0,04	0,04	0,03	0,04	0,04
VCAM-1	0,07	0,08	0,21	0,13	0,04	0,04